INTERNATIONAL JOURNAL FOR NUMERICAL METHODS IN ENGINEERING
*Int. J. Numer. Meth. Engng* 2001; **52**:921–938 (DOI: 10.1002/nme.239)

# Topological aspects of meshless methods and nodal ordering for meshless discretizations

Arash Yavari[1,†], Ali Kaveh[2], Shahram Sarkani[1,*,‡]
and Hosein Ali Rahimi Bondarabady[3]

[1]*School of Engineering and Applied Science, The George Washington University, Washington, DC 20052, U.S.A.*
[2]*Iran University of Science and Technology, Narmak, Tehran 16, Iran*
[3]*Department of Civil Engineering, University of Yazd, Yazd, Iran*

SUMMARY

The meshless element-free Galerkin method (EFGM) is considered and compared to the finite-element method (FEM). In particular, topological aspects of meshless methods as the nodal connectivity and invertibility of matrices are studied and compared to those of the FE method. We define four associated graphs for meshless discretizations of EFGM and investigate their connectivity. The ways that the associated graphs for coupled FE-EFG models might be defined are recommended. The associated graphs are used for nodal ordering of meshless models in order to reduce the bandwidth, profile, maximum frontwidth, and root-mean-square wavefront of the corresponding matrices. Finally, the associated graphs are numerically compared. Copyright © 2001 John Wiley & Sons, Ltd.

KEY WORDS: meshless methods; nodal ordering; graph theory

## 1. INTRODUCTION

The finite-element method (FEM) is a numerical method that has been most widely used in solid mechanics for the last three decades. Nowadays most analysis softwares are based on this numerical technique. Yet, this method, while being very efficient, has some drawbacks. For one, mesh generation is very time-consuming and expensive especially for three-dimensional problems. The finite-element method is not efficient for solving problems such as crack

*Correspondence to: Shahram Sarkani, School of Engineering and Applied Science, Office of the Associate Dean for Research and Development, The George Washington University, Tompkins Hall, 725 23rd Ste. N.W., Ste. 109, Washington, DC 20052, U.S.A.
†Currently at the Graduate Aeronautical Laboratories, California Institute of Technology, Pasadena, CA 91125, U.S.A.
‡sarkani@seas.gwu.edu

*Received 1 November 1999*
*Revised 9 October 2000*

propagation or large deformations for which remeshing is required in each step of the analysis. Numerical methods for which data preparation is less expensive, are more attractive for these classes of problems.

In recent years several meshless methods have appeared in the literature. These methods do not require any fixed connectivity information such as mesh. In these methods the discrete model is completely represented by nodes and a description of the boundary. Different meshless methods have different interpolation constructions, but they have many properties in common.

Lucy [1] in 1977 introduced the first meshless method. Calling it the smooth particle hydrodynamics method, he used it to model astrophysical phenomena without boundaries. In the literature, meshless methods have also been referred to as gridless, element-free, clouds, point element, and diffuse elements. Among the many meshless methods we can mention are: particle-in-cell methods [2], diffuse-element methods [3], h–p clouds [4], the particle-of-unity-finite element method [5], wavelet particle methods [6, 7], and reproducing-kernel-particle methods [6–8].

It is worth mentioning that one of the disadvantages of meshless methods is the difficulty of applying essential boundary conditions. Belytschko *et al.* [9], enforced essential boundary conditions for their element-free Galerkin method by using Lagrange multipliers. Lu *et al.* [10], applied geometric boundary conditions using a modified variational principle. Krongauz and Belytschko [11] enforced the essential boundary conditions by inserting a string of finite elements along the essential boundary.

Using meshless methods leads, as do other numerical techniques, to solving a very large system of linear equations:

$$\mathbf{Kx} = \mathbf{f}$$

Traditional methods of solving systems of linear equations are not efficient for practical engineering problems; the matrix $\mathbf{K}$ is highly sparse and special numerical techniques should be used to solve these equations. For an efficient analysis, band, profile, and frontal methods are widely used. There have been many investigations into ordering nodes and elements so as to yield optimal or near-optimal banded matrices or matrices with the lowest possible profiles. There is a variety of procedures for optimally analysing structures using displacement or force methods. Some of these ordering methods are graph theoretical. When using graph theory in these classes of methods, connectivity properties of a finite-element model or those of a skeletal structure are transformed into the topological properties of graphs.

Cuthill and McKee [12] were the first to use graph theory to reduce the bandwidth of stiffness matrices for skeletal structures. Kaveh [13, 14] offered a two-step method for nodal ordering using a shortest route tree. For ordering finite-element nodes, different methods have been developed to date. The corner node method was introduced by Cassell *et al.* [15], and by Kaveh and Rahimi Bondarabadi [16]. Kaveh [13, 14] and Fenves and Law [17] applied a natural associated graph in a two-step approach. Sloan [18] and Livesley and Sabin [19] used an element clique graph. Kaveh [20] defined a connectivity co-ordinate system for node and element ordering. Kaveh and Behfar [21] defined five different graphs for the connectivity of FE models for finite-element nodal ordering and compared them. Kaveh and Roosta [22] presented nine different graphs for representing the connectivity of FE models and compared them numerically.

 

As for existing numerical methods, having efficient solution procedures for meshless methods is crucial. These methods seem to be practically useful and in the near future they will be used in practical applications. Therefore, an investigation of nodal ordering for meshless discretizations is of great practical importance. In this article, we study some topological aspects of meshless methods and define some associated graphs for nodal ordering. It should be noted that if we have a good understanding of the topology of a meshless model, appropriate associated graphs can be defined. Having an appropriate associated graph that describes the topology of the model correctly, any of the excising nodal ordering algorithms can be utilized. In this paper, we will not discuss those nodal ordering algorithms.

This article is organized as follows. In Section 2 the element-free Galerkin method (EFGM) is reviewed and its nodal connectivity is discussed and compared with that of the finite-element method (FEM). Section 3 addresses some issues regarding the invertibility of the relevant matrices. In Section 4, four associated graphs are defined for meshless discretizations and the possible ways of defining graphs for coupled FE-EFGM are discussed. In Section 5 nodal ordering methods for meshless discretizations are introduced. In Section 6 some numerical examples are solved and the associated graphs are numerically compared. Conclusions are given in Section 7.

## 2. THE ELEMENT-FREE GALERKIN METHOD

The element-free Galerkin method is a meshless method that uses a moving least-squares approximation. Nayroles *et al.* [3], the first to use a moving least-squares approximation in a Galerkin method, called it the diffuse-element method. The interpolants used in this method had been introduced and investigated earlier by Lancaster and Salkauskas [23]. Later the method was modified by Belytschko *et al.* [9], and called the element-free Galerkin method. The concepts we introduce in the present section follow Belytschko *et al.* [9], and Belytschko *et al.* [24].

### *2.1. Moving least-squares approximation*

The element-free Galerkin method uses moving least-squares interpolants. Moving least-squares require only nodes for constructing shape functions. Here, our goal is to approximate a function $\mathbf{u}(\mathbf{x})$ in the domain $\Omega$. According to the moving least-squares method, $\mathbf{u}(\mathbf{x})$ is approximated by $\mathbf{u}^{\mathrm{h}}(\mathbf{x})$ as

$$u^{\mathrm{h}}(\mathbf{x}) = \sum_{i=1}^{m} p_i(\mathbf{x}) a_i(\mathbf{x}) = \mathbf{p}^{\mathrm{T}}(\mathbf{x})\mathbf{a}(\mathbf{x}) \tag{1}$$

where $p_i(\mathbf{x})$ are monomial basis functions, $a_i(\mathbf{x})$ are some coefficients which are functions of $\mathbf{x}$, and $m$ is the number of terms in the basis. For example,

$$\mathbf{p}^{\mathrm{T}}(\mathbf{x}) = (1, x, x^2, \ldots, x^m) \quad \text{in 1D} \tag{2a}$$

$$\mathbf{p}^{\mathrm{T}}(\mathbf{x}) = (1, x, y, x^2, xy, y^2, \ldots, y^m) \quad \text{in 2D} \tag{2b}$$

 

We can obtain the unknown coefficients $a_i(\mathbf{x})$ at any point $\mathbf{x}$ by performing a weighted least-squares fit; i.e., by minimizing the following discrete $L_2$ norm:

$$J = \sum_{I=1}^{n} w(\mathbf{x} - \mathbf{x}_I) \left[\mathbf{p}^{\mathrm{T}}(\mathbf{x}_I)\mathbf{a}(\mathbf{x}) - u_I\right]^2 \tag{3}$$

where $\mathbf{x}_I$ and $u_I$ are the respective nodal co-ordinates and nodal values of $u$, $w(\mathbf{x} - \mathbf{x}_I)$ are weight functions, and $n$ is the number of nodes in the neighbourhood of $\mathbf{x}$ for which the weight function $w(\mathbf{x} - \mathbf{x}_I)$ is non-zero. The weight functions $w(\mathbf{x} - \mathbf{x}_I)$ have compact supports; i.e., $w(\mathbf{x} - \mathbf{x}_I)$ is non-zero only in a subdomain $\Omega_I$ of $\Omega$. The subdomain $\Omega_I$ is called the domain of influence of the node $I$.

Minimizing $J$ with respect to $a(\mathbf{x})$ yields:

$$\mathbf{a}(\mathbf{x}) = \mathbf{A}^{-1}(\mathbf{x})\mathbf{B}(\mathbf{x})\mathbf{u} \tag{4}$$

where

$$\mathbf{A}(\mathbf{x}) = \sum_{I=1}^{n} w(\mathbf{x} - \mathbf{x}_I)\, p(\mathbf{x}_I)\, p^{\mathrm{T}}(\mathbf{x}_I) \tag{5a}$$

$$\mathbf{B}(\mathbf{x}) = (w(\mathbf{x} - \mathbf{x}_1)\mathbf{p}(\mathbf{x}_1), w(\mathbf{x} - \mathbf{x}_2)\mathbf{p}(\mathbf{x}_2), \ldots, w(\mathbf{x} - \mathbf{x}_n)\, p(\mathbf{x}_n)) \tag{5b}$$

$$\mathbf{u}^{\mathrm{T}} = (u_1, u_2, \ldots, u_n) \tag{5c}$$

Obviously, for (4) to be meaningful, $\mathbf{A}(\mathbf{x})$ must be invertible. Substituting (4) into (1), we obtain

$$u^{\mathrm{h}}(\mathbf{x}) = \sum_{I=1}^{n} \sum_{i=1}^{m} p_i(\mathbf{x})(\mathbf{A}^{-1}(\mathbf{x})\mathbf{B}(\mathbf{x}))_{iI} u_I = \sum_{I=1}^{n} \Phi_I(\mathbf{x}) u_I \tag{6}$$

where shape functions are defined as

$$\Phi_I(\mathbf{x}) = \sum_{I=1}^{m} p_j(\mathbf{x})(\mathbf{A}^{-1}(\mathbf{x})\mathbf{B}(\mathbf{x}))_{jI} \tag{7}$$

It should be noted that these shape functions, generally, do not satisfy the Kronecker delta criterion, i.e., $\Phi_I(x_J) \neq \delta_{IJ}$. Generalization of the above idea for obtaining continuous moving least-squares approximations is straightforward.

As was shown by Belytschko *et al.* [9], for the two-dimensional elasto-static problem

$$\nabla . \sigma + \mathbf{b} = \mathbf{0} \quad \text{in } \Omega \tag{8a}$$

$$\sigma . \mathbf{n} = \bar{\mathbf{t}} \quad \text{on } \partial\Omega_t \tag{8b}$$

$$\mathbf{u} = \bar{\mathbf{u}} \quad \text{on } \partial\Omega_u \tag{8c}$$

the element-free Galerkin method yields the following discrete equations:

$$\begin{bmatrix} \mathbf{K} & \mathbf{G} \\ \mathbf{G}^{\mathrm{T}} & \mathbf{0} \end{bmatrix} \begin{Bmatrix} \mathbf{u} \\ \boldsymbol{\lambda} \end{Bmatrix} = \begin{Bmatrix} \mathbf{f} \\ \mathbf{q} \end{Bmatrix} \tag{9}$$

 

where $\boldsymbol{\lambda}$ are Lagrange multipliers for satisfying essential boundary conditions, and $\mathbf{f}$ and $\mathbf{q}$ are force terms. The matrix $\mathbf{G}$ results from the use of Lagrange multipliers method. Here, only the explicit form of $\mathbf{K}$ is important for our purposes. The matrix $\mathbf{K}$ may be expressed as

$$\mathbf{K}_{IJ} = \int_{\Omega} \mathbf{B}_I^{\mathrm{T}} \mathbf{D} \mathbf{B}_J^I \, \mathrm{d}\Omega \tag{10}$$

where

$$\mathbf{B}_I = \begin{bmatrix} \Phi_{I,x} & 0 \\ 0 & \Phi_{I,y} \\ \Phi_{I,y} & \Phi_{I,x} \end{bmatrix} \tag{11a}$$

and

$$\mathbf{D} = \frac{E}{1-v^2} \begin{bmatrix} 1 & v & 0 \\ 0 & 1 & 0 \\ 0 & 0 & (1-v)/2 \end{bmatrix} \quad \text{(plane stress)} \tag{11b}$$

### 2.2. Node connectivity in EFGM

For the sake of simplicity, consider a 2-D elastic body. By definition, we know that

$$\Phi_I(\mathbf{x}) \neq 0 \quad \Leftrightarrow \quad \mathbf{x} \in \Omega_I \tag{12}$$

Hence from (11a):

$$\mathbf{B}_I(\mathbf{x}) \neq \mathbf{0} \quad \Leftrightarrow \quad \mathbf{x} \in \Omega_I \tag{13}$$

Now considering two nodes $I$ and $J$, we have

$$\mathbf{B}_I \neq \mathbf{0} \quad \Leftrightarrow \quad \mathbf{x} \in \Omega_I \quad \text{and} \quad \mathbf{B}_J \neq \mathbf{0} \quad \Leftrightarrow \quad \mathbf{x} \in \Omega_J \tag{14a}$$

Hence

$$\mathbf{B}_I^{\mathrm{T}} \mathbf{D} \mathbf{B}_J \neq \mathbf{0} \quad \Leftrightarrow \quad \Omega_I \cap \Omega_J \neq \emptyset \tag{14b}$$

Comparing (10) and (14b), we have

$$\mathbf{K}_{IJ} \neq \mathbf{0} \quad \Leftrightarrow \quad \Omega_I \cap \Omega_J \neq \emptyset \tag{15}$$

In summary, nodes $I$ and $J$ are connected if and only if their domains of influence have a non-empty intersection with non-zero area. It should be noted that it is possible that $I \notin \Omega_J$ or $J \notin \Omega_I$ when $I$ and $J$ are connected, as is shown in Figure 1. Here we consider disk-shaped domains of influence.

In a finite-element mesh the domain of influence of a node $I$ may be expressed by

$$\Omega_I = \bigcup_{j=1}^{M} E_j \tag{16}$$

where the $E_j$'s are elements that contain node $I$, and $M$ is the number of such elements. An example is shown in Figure 2. In a finite-element mesh two nodes $I$ and $J$ are connected

 

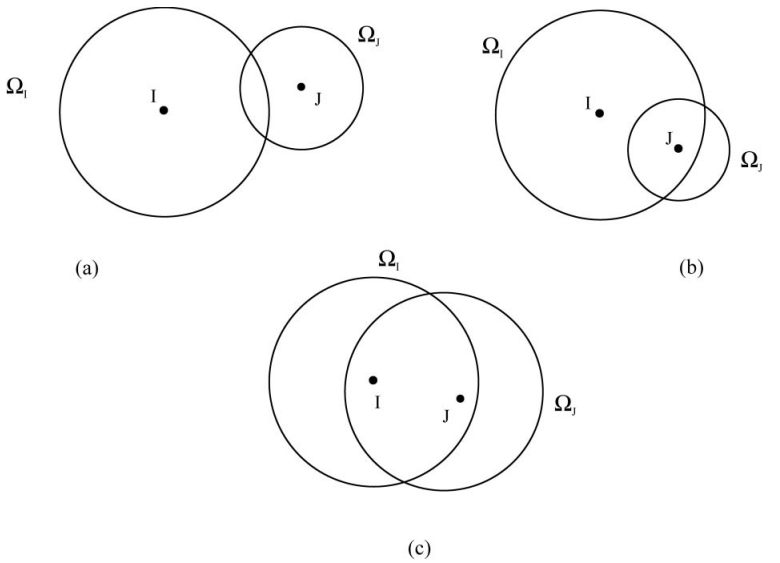


Figure 1. Two nodes and their domains of influence ($\Omega_I \cap \Omega_J \neq \emptyset$): (a) $I \notin \Omega_J,\ J \notin \Omega_I$; (b) $I \notin \Omega_J,\ J \in \Omega_I$; (c) $I \in \Omega_J,\ J \in \Omega_I$.

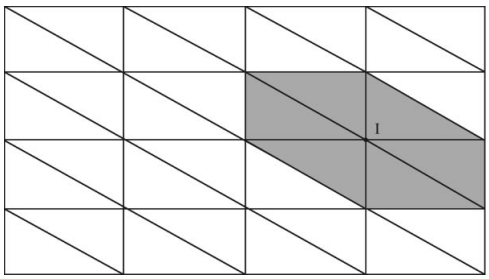


Figure 2. Domain of influence of a typical node in a finite element mesh.

if and only if both belong to at least one element, or in other words, if their domains of influence have a non-empty intersection with non-zero area. Note that in this case:

$$I \in \Omega_J \ \Leftrightarrow\ J \in \Omega_I \tag{17}$$

Therefore, the connectivity of nodes is similar in the two methods. However, (17) holds only for the finite-element method. As is depicted in Figure 1, (17) is not generally valid for meshless models. This creates some new problems, which will be discussed in later sections.

Usually, in a meshless model all domains of influence have the same shape; for example, they are all disk-shaped or rectangular. But in a finite-element model, the shapes of the domains of influence differ for different nodes.

 

## 3. THE INVERTIBILITY OF STRUCTURAL MATRICES

Suppose that $q$ is the number of non-zero weights at a point $\mathbf{x}$, and $m$ is the number of terms in the basis. For $\mathbf{A}(\mathbf{x})$ to be invertible we must have, $q \geqslant m$ [11]. Practically, domains of influence of the nodes are chosen large enough to have non-singular $\mathbf{A}$ matrix at any point $\mathbf{x}$. Clearly, the only parameter that can be controlled for a meshless model is the size of the domains of influence. Now consider a 2-D meshless discretization.

We want to have at least $m$ non-zero weights at any point and in particular at any node. A bipartite graph is defined as follows: The sets A and B are sets of nodes and corresponding domains of influence. A node $I \in A$ is adjacent to a node $J \in B$ if and only if $I \in \Omega_J$. Thus, we want each node in A to be adjacent to at least $m$ nodes in $B$. If each domain of influence contains at least $m$ nodes, or in other words if each node in $B$ is adjacent to at least $m$ nodes in $A$, we cannot conclude that each node in $A$ is also adjacent to at least $m$ nodes in $B$. Hence, we cannot conclude that there are at least $m$ non-zero weights at each node, and consequently nothing can be said about an arbitrary point. The problem is that, in addition to the topological properties, the geometry of the discretized system must be taken into account. This dependence on the geometric configuration of the discretization makes meshless methods more complicated than the finite-element method; however, practically, domains of influence are chosen large enough and the distribution of nodes is almost uniform. For such models all the relevant matrices are invertible.

Now consider a system of uniformly spaced nodes as shown in Figure 3. Using the symmetry of the domain, it is enough to consider the square ABCD in Figure 3. First, assume that the sizes of the domains of influence are a little larger than the smallest distance between neighbouring nodes. Assume that the domains of influence are disk-shaped. Considering this size for domains of influence, each domain of influence contains five nodes. Also assume that a linear basis is used ($m = 3$).

As is shown in Figure 3, the square ABCD is partitioned into three subdomains, $\Omega_a$, $\Omega_b$, and $\Omega_c$. For any point in $\Omega_a$ there are four non-zero weights, for any point in $\Omega_b$ there are three non-zero weights, and for any point in $\Omega_c$ there are two non-zero weights. Therefore, the matrix $\mathbf{A}$ is singular for all points in $\Omega_c$. Each domain of influence contains five nodes but there are points for which there are only two non-zero weights. Suppose that $c_I$ is the distance between $I$ and the nearest-neighbouring node, and $d_{\max}$ is the size of the domain of influence of node $I$. All investigators have considered the following relation:

$$d_{\max} = d_m c_I \tag{18}$$

where $2 \leqslant d_m \leqslant 4$. Clearly, for the uniformly spaced nodes, with $d_m = 2$ at any point there will be more than three non-zero weights, and hence the basis is satisfied.

Now consider meshless discretization in one dimension. In this case the domain is a line segment. Assume that a linear basis is used ($m = 2$). For $\mathbf{A}$ to be invertible, at any point of the domain we must have $n \geqslant m$ non-zero weights ($n \geqslant 2$). Dolbow and Belytschko [25] mention that if a given node has only one neighbouring node in its domain of influence, $\mathbf{A}$ will be singular, and so each node must have at least two neighbouring nodes in its domain of influence for $\mathbf{A}$ to be invertible.

Suppose that each node has two neighbouring nodes in its domain of influence. Hence, any node I belongs to $\Omega_{I-1}$, $\Omega_I$ and $\Omega_{I+1}$. If $I$ is a boundary point, it belongs to $\Omega_I$ and $\Omega_{I+1}$ or $\Omega_{I-1}$ and $\Omega_I$. Consider nodes $I$ and $I+1$. If neither of them is a boundary point, for each

 

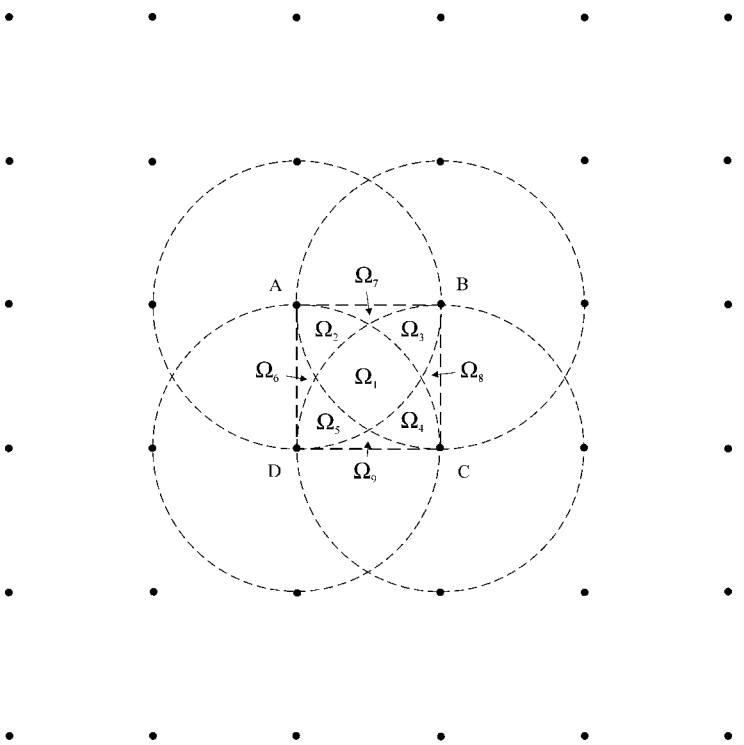


$$\Omega_a = \Omega_1, \quad \Omega_b = \Omega_2 \cup \Omega_3 \cup \Omega_4 \cup \Omega_5, \quad \Omega_c = \Omega_6 \cup \Omega_7 \cup \Omega_8 \cup \Omega_9$$

Figure 3. A uniformly spaced system of nodes.

point in the interval $(I, I+1)$ there are four non-zero weights. If $I$ or $I+1$ is a boundary point, for any point in the interval $(I, I+1)$ there are three non-zero weights. Therefore, the simplicity of the 1-D discretizations allows us to reach the following conclusion: if a $k$th-order basis is used ($m = k+1$), $\mathbf{A}$ is invertible if each node has at least $k+1$ neighbouring nodes in its domain of influence.

As was mentioned earlier in this section, nothing conclusive can be said about the required sizes of the domains of influence for a general meshless model. The only thing that can be done is to choose large domains of influence. However, when meshless nodes are non-uniformly distributed in the domain non-uniform sizes for the domains of influence can be used. This way we will have a more efficient discretization than a discretization with uniform domains of influence. Experience has shown that for practical purposes, with linear bases, $2 \leqslant d_m \leqslant 4$ is enough. Another interesting qualitative conclusion is that for this reason, usually matrices resulting from finite-element discretizations are sparser. Hence, the finite-element method is more attractive from this point of view.

 

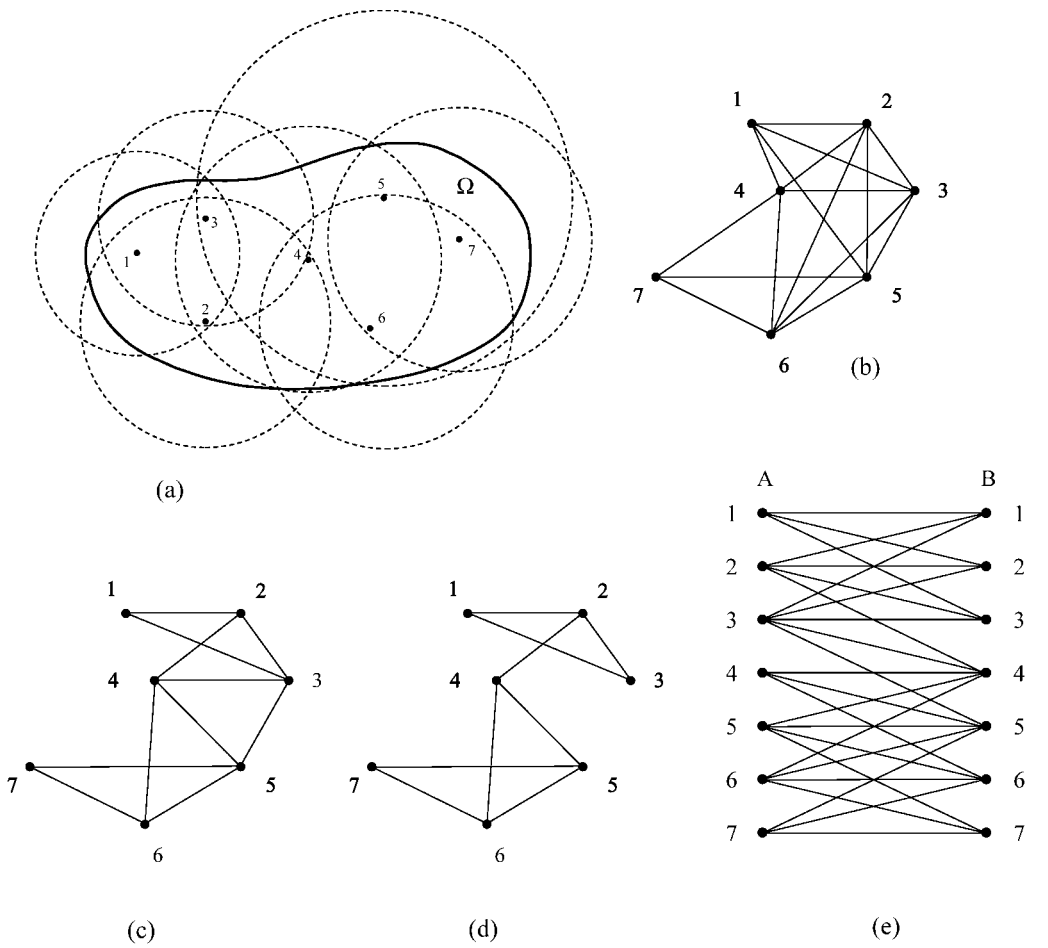


Figure 4. (a) A meshless model with seven nodes; (b) SCAG; (c) PCAG; (d) WCAG; (e) ABG.

## 4. ASSOCIATED GRAPHS FOR A MESHLESS MODEL

In this section we define four associated graphs for an EFGM discretization. These graphs represent the connectivity of a meshless model. Consider the domain shown in Figure 4a. The meshless model consists of seven nodes with the domains of influence as shown. For the sake of clarity, the associated graphs are shown for this example model. The associated graphs are defined as follows:

1. *Strongly Connected Associated Graph* (*SCAG*): The SCAG of a meshless model is a graph whose nodes are the same as those of the meshless model; two nodes $n_i$ and $n_j$ of SCAG are connected with a member if and only if $\Omega_I \cap \Omega_J \neq \emptyset$ in the meshless model. Figure 4b shows the strongly connected associated graph for the meshless model of Figure 4a.
2. *Partially Connected Associated Graph* (*PCAG*): The PCAG of a meshless model is a graph whose nodes are also the same as those of the meshless model; here two nodes $n_i$ and

 

$n_j$ of PCAG are connected with a member if and only if $I \in \Omega_J$ *or* $J \in \Omega_I$ in the meshless model. Figure 4c shows the partially connected associated graph for the meshless model of Figure 4a.

3. *Weakly Connected Associated Graph* (*WCAG*): The WCAG of a meshless model is a graph whose nodes are again the same as those of the meshless model; in this case two nodes $n_i$ and $n_j$ of WCAG are connected with a member if and only if $I \in \Omega_J$ *and* $J \in \Omega_I$ in the meshless model. Figure 4d shows the weakly connected associated graph for the meshless model of Figure 4a.

4. *Associated Bipartite Graph* (*ABG*): The ABG has two sets, A and B, corresponding to nodes and domain of influence, respectively. A node $n_i \in$ A is connected to $n_j \in$ B by a member if and only if $I \in \Omega_J$. Figure 4e shows the associated bipartite graph for the meshless model of Figure 4a. This graph was defined earlier in Section 3.

We now prove that the strongly connected associated graph defined above is always a connected graph.

*Lemma.* If a meshless model satisfies the basis, i.e., at any point there are at least $m$ non-zero weights, the strongly connected associated graph SCAG is connected.

*Proof.* The lemma is proved by contradiction. Assume that SCAG is disconnected; for example, it is composed of two disjoint subgraphs $SCAG_1$ and $SCAG_2$. This means that $\Omega$ can be partitioned into three subdomains, $\Omega_1$, $\Omega_2$, and $\Omega_3$, such that there are points in $\Omega_3$ with no non-zero weight. This contradiction shows that SCAG must be connected.

It is to be noted that this lemma is not generally valid for the other three associated graphs. Suppose that the domain $\Omega$ can be partitioned into three subdomains, $\Omega_1$, $\Omega_2$, and $\Omega_3$, such that there is no node in $\Omega_3$. However, we can have $m$ non-zero weights at each point of $\Omega_3$ such that no node in $\Omega_2$ belongs to any domain of influence of the nodes of $\Omega_1$, and vice versa. This model can generally satisfy the basis, i.e., all the relevant matrices are invertible. However, the corresponding PCAG, WCAG, and ABG are not connected graphs. Even if the associated graphs are disconnected, we can make them connected graphs by adding some members. Obviously, for such cases SCAG gives a better nodal ordering. The possible disconnectedness of these associated graphs does not mean that we should rule them out. In practical problems, the meshless model consists of an almost uniform distribution of nodes. Such a meshless model usually has connected associated graphs. PCAG and WCAG usually have fewer elements compared to SCAG, which makes them more attractive for our purposes.

### *4.1. Associated graphs for a coupled FE-EFGM model*

It is known that, generally, the finite-element method is more efficient than meshless methods. Meshless methods are more efficient only for problems in which remeshing is needed if they are analysed by the finite-element method. Usually remeshing is needed only for a subdomain of the problem. Therefore, a more economical analysis is to solve the problem by a combination of finite-element and meshless methods. Belytschko *et al.* [26], developed a coupled finite-element element-free Galerkin method and applied it to crack propagation problems. They used meshless discretizations around cracks and finite elements for the rest of

 

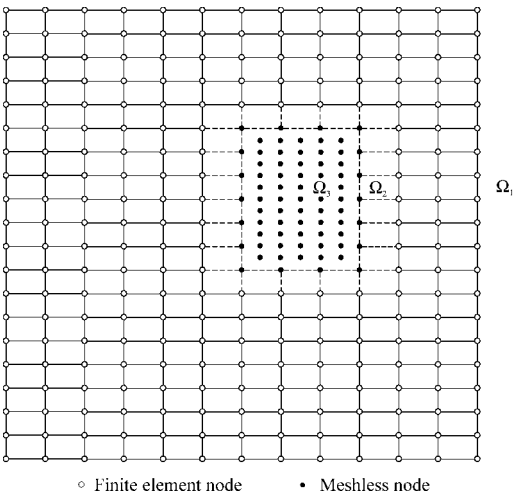


Figure 5. A coupled finite-element meshless model.

the domain. By this method the domain $\Omega$ is partitioned into three subdomains, $\Omega_1$, $\Omega_2$, and $\Omega_3$. In $\Omega_1$ and $\Omega_3$ finite elements and meshless approximations are used, respectively, and $\Omega_2$ is the transition domain with interface elements (Figure 5).

For finite-element nodes in $\Omega_1$, any of the nine associated graphs defined in Reference [22] can be considered. For the meshless discretized subdomain $\Omega_2$ we can consider the strongly, weakly, or partially connected associated graphs. Interface elements in $\Omega_3$ are treated like finite elements; a meshless node is connected to a finite-element node if they belong to the same interface element. An example is shown in Figure 6.

## 5. NODAL ORDERING FOR MESHLESS DISCRETIZATION

Meshless methods seem to be very promising for future engineering applications. Therefore appropriate node ordering for these methods is very important in practice. In Belytschko *et al.* [9], we read: "If the nodes are numbered judiciously, for example, by sorting the $x$-co-ordinates, the **K** part of the matrix in Equation (28) will be banded". Their Equation (28) is the same as Equation (9) in this paper. In this section we propose techniques for answering this question more precisely.

For ordering a meshless discretization, first an associated graph is defined to describe the topology of the meshless model. Then ordering is performed for this graph using any of the algorithms in the literature. If SCAG, PCAG, or WCAG are ordered, the final node ordering is found simply by assigning the same numbering to the corresponding nodes of the meshless model. And if ABG is used, after ordering the nodes of the graph we omit all the nodes of the set B (corresponding to the domains of influence). This way nodes in A are numbered $n_1, n_2, n_3, \ldots$, where $n_1 < n_2 < n_3 < \ldots$ . Then the nodes are renumbered according to $n_1 \rightarrow 1,\ n_2, \rightarrow 2,\ n_3 \rightarrow 3, \ldots$ . Finally, the same numbering is assigned to the corresponding nodes of the meshless model.

 

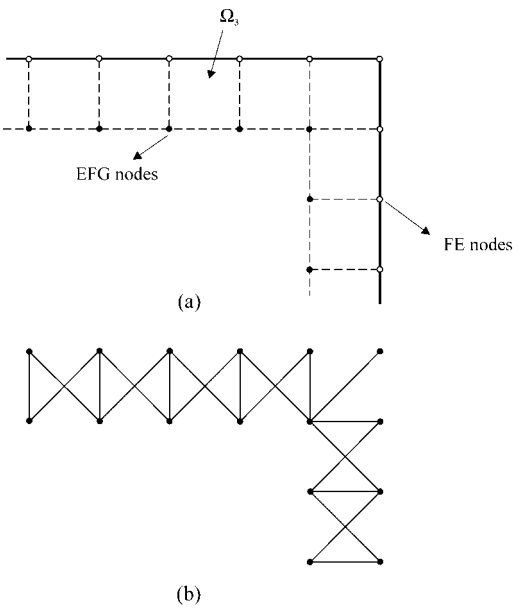


Figure 6. (a) Transition subdomain; and (b) its associated graph.

In the next section nodal ordering is performed for some meshless models and the four associated graphs are compared numerically.

## 6. NUMERICAL EXAMPLES

Here the four associated graphs are used for the nodal ordering of four different meshless models. In all these examples Sloan's algorithm [27] is utilized for ordering. The bandwidth ($B$), profile ($P$), maximum frontwidth ($F_{\max}$), and the root-mean-square wavefront ($F_{\text{rms}}$) are calculated for each model. For two of the examples, four-noded finite elements with the same nodal points are considered and the results are compared with those of meshless discretizations. For the sake of self-containedness, a few definitions are given here. For more details the reader may refer to References [28, 29].

The *half bandwidth* of the $i$th row of an $N \times N$ matrix $\mathbf{K}$ is defined as

$$b_i = i - j_{\min}(i) + 1 \tag{19}$$

where $j_{\min}(i)$ is the smallest index $j$ in the $i$th row for which $k_{ij} \neq 0$. The *half bandwidth* of matrix $\mathbf{K}$ is defined as

$$B = \max_i b_i \tag{20}$$

and

$$P = \sum_{i=1}^{N} b_i \tag{21}$$

 

Table I. Minimum $d_m$ values for having connected graph models.

| Graph model | SCAG | PCAG | WCAG | ABG |
|---|---|---|---|---|
| Example 1 | 1.5 | 2.5 | 4.1 | 2.5 |
| Example 2 | 1.0 | 1.0 | 3.0 | 1.0 |
| Example 3 | 1.0 | 1.5 | 2.5 | 1.5 |
| Example 4 | 1.0 | 1.0 | 1.0 | 1.0 |

is the *profile* of the matrix **K**. The column $j$ is said to be active at stage $i$, if $j \geqslant i$ and there is a non-zero entry in column $j$ with a row index $k$ such that $k \geqslant i$. Let $f_i$ denote the number of columns that are active at stage $i$, then the maximum *frontwidth* of $k$ is defined as

$$F_{\max} = \max_i f_i \tag{22}$$

The *root-mean-square wavefront* is defined as

$$F_{\text{rms}} = \sqrt{\frac{1}{N} \sum_{i=1}^{N} f_i^2} \tag{23}$$

For each example, $d_m$ is assumed to be the same for all the nodes of the model. A small $d_m$ value can lead to disconnected graph models, which is not desirable. The minimum $d_m$ values for each example and each graph model are shown in Table I. As can be seen, WCAG has the weakest connectivity and always needs larger $d_m$'s than the other graph models do in order to stay connected. Also, SCAG has the strongest connectivity and thus needs smaller $d_m$'s than other graph models do in order to stay connected.

For each example, we chose the same value of $d_m$ for all graph models so as to compare them. Therefore, for each example, we must choose the maximum $d_m$ to make sure that all the graph models are connected. We choose $d_m = 4.1$, 3.0, 2.5, and 2.0 for examples 1, 2, 3, and 4, respectively. In practical problems, we might be required to perform a nodal ordering for a meshless model that has some disconnected graph models. In that case, we can make the disconnected graphs connected graphs by adding some new members.

*Example 1.* This example considers one-fourth of a rectangular plate with a circular hole [9]. The meshless model is shown in Figure 7. This model contains 54 nodes, and $d_m = 4.1$ is selected. The bandwidths, profiles, maximum frontwidths, and the root-mean-square wavefronts calculated using the four associated graphs are shown in Table II(a). It may be seen that the four graphs give almost the same $B$, $P$, $F_{\max}$, and $F_{\text{rms}}$. This is because a large $d_m$ $(=4.1)$ has been used for this example and all the graph models are nearly complete.

*Example 2.* This example considers one-half of an edge-cracked plate [9]. The meshless model is shown in Figure 8. This model contains 154 nodes, and $d_m = 3.0$ is selected. The bandwidths, profiles, maximum frontwidths, and the root-mean-square wavefronts are given in Table II(b). It may be seen that for this configuration WCAG gives the smallest $B$ and SCAG gives the smallest $P$, $F_{\max}$, and $F_{\text{rms}}$.

 

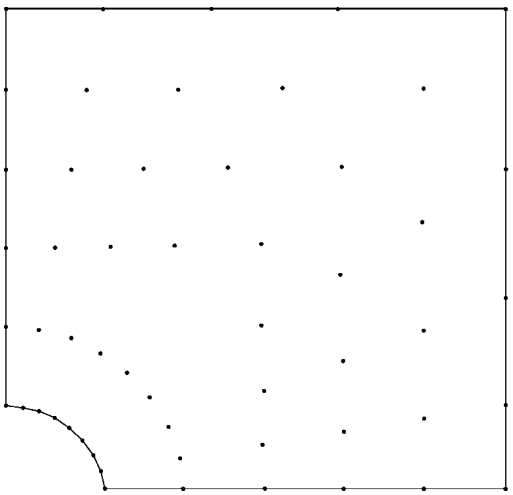

Figure 7. Meshless discretization of a square plate with a circular hole with 54 nodes (after Belytschko *et al.* [9]).

Table II.

| Graph model | SCAG | PCAG | WCAG | ABG |
|---|---|---|---|---|
| (a) Results of Example 1 ($d_m = 4.1$) | | | | |
| No. of members | 1343 | 1325 | 404 | 867 |
| $B$ | 49 | 51 | 51 | 51 |
| $P$ | 1428 | 1456 | 1423 | 1430 |
| $F_{max}$ | 45 | 49 | 45 | 46 |
| $F_{rms}$ | 30.1 | 30.8 | 29.9 | 30.1 |
| (b) Results of Example 2 ($d_m = 3.0$) | | | | |
| No. of elements | 5084 | 3715 | 1428 | 2133 |
| $B$ | 121 | 101 | 96 | 117 |
| $P$ | 6606 | 8017 | 7458 | 8547 |
| $F_{max}$ | 63 | 82 | 75 | 89 |
| $F_{rms}$ | 46.0 | 56.4 | 52.2 | 61.1 |
| (c) Results of Example 3 ($d_m = 2.5$) | | | | |
| No. of elements | 20228 | 12603 | 5688 | 6176 |
| $B$ | 449 | 450 | 422 | 430 |
| $P$ | 58279 | 61208 | 61384 | 58514 |
| $F_{max}$ | 130 | 144 | 138 | 136 |
| $F_{rms}$ | 83.4 | 88.5 | 88.2 | 84.0 |
| (d) Results of Example 4 ($d_m = 2.0$) | | | | |
| No. of elements | 18028 | 10648 | 4884 | 4884 |
| $B$ | 267 | 169 | 161 | 161 |
| $P$ | 69576 | 75862 | 75924 | 75924 |
| $F_{max}$ | 110 | 113 | 113 | 113 |
| $F_{rms}$ | 82.1 | 82.9 | 90.0 | 90.0 |

 

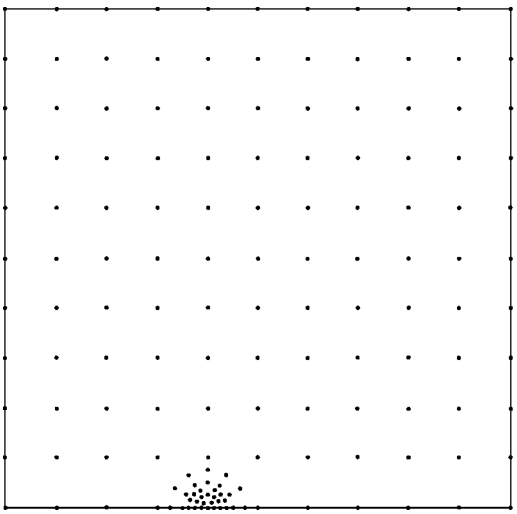

Figure 8. Meshless discretization of an edge-cracked plate with 154 nodes (after Belytschko *et al.* [9]).

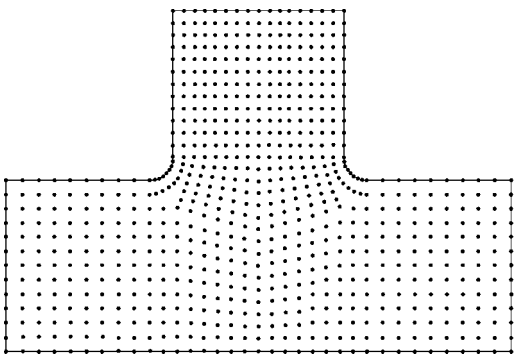

Figure 9. Meshless discretization for the problem of a crack path propagation from a fillet for the case of a thin I-beam with 739 nodes (after Belytschko *et al.* [24]).

*Example 3.* In this example, the meshless discretization for the problem of a crack path propagation from a fillet for the case of a thin I-beam [24] is considered. The meshless model of this example is shown in Figure 9. This model contains 739 nodes, and the value for $d_m$ is 2.5. The bandwidths, profiles, maximum frontwidths, and the root-mean-square wavefronts are given in Table II(c), where WCAG shows the smallest $B$ while SCAG gives the smallest $P$, $F_{max}$, and $F_{rms}$.

*Example 4.* This example considers a square plate with a square hole. The meshless model is shown in Figure 10. This model contains 880 nodes, and $d_m = 2.0$ is selected. Table II(d) shows the bandwidths, profiles, maximum frontwidths, and the root-mean-square wavefronts. For this configuration WCAG and ABG give the smallest value for $B$ and SCAG gives the smallest $P$, $F_{max}$, and $F_{rms}$.

 

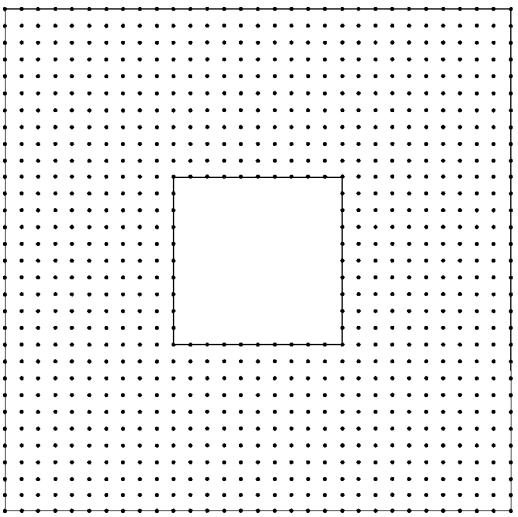

Figure 10. Meshless discretization of a square plate with a square hole with 880 nodes.

Table III.

| Model | $B$ | $P$ | $F_{\max}$ | $F_{\text{rms}}$ |
|---|---|---|---|---|
| (a) Comparison between EFGM and EF for Example 1 | | | | |
| Meshless (avg) | 50.50 | 1434.25 | 46.25 | 30.22 |
| Finite element | 15.00 | 37.60 | 9.00 | 7.20 |
| MLS/FE | 3.37 | 3.81 | 5.14 | 4.20 |
| (b) Comparison between EFGM and EF for Example 4 | | | | |
| Meshless (avg) | 189.50 | 74321.50 | 112.25 | 86.25 |
| Finite element | 138.00 | 24980.00 | 56.00 | 30.70 |
| MLS/FE | 1.37 | 2.97 | 2.00 | 2.81 |

*Comparison with FE*: For comparing Meshless and finite-element discretizations, in Examples 1 and 4 rectangular four-noded finite elements are considered and $B$, $P$, $F_{\max}$, and $F_{\text{rms}}$ are calculated. For Example 1, considering four-noded finite elements with the same nodal points as in Figure 7, the magnitudes of $B$, $P$, $F_{\max}$, and $F_{\text{rms}}$ of the stiffness matrix are obtained as 15, 376, 9, and 7.2, respectively. Similarly, for Example 4 considering rectangular four-noded finite elements with the same nodal points as in Figure 10, the magnitude of $B$, $P$, $F_{\max}$, and $F_{\text{rms}}$ of the stiffness matrix are obtained as 138, 24980, 56, and 30.7, respectively. The results are compared with those of meshless discretizations in Tables III(a) and III(b). In these tables the average values of $B$, $P$, $F_{\max}$, and $F_{\text{rms}}$ obtained from the four different associated graphs are considered for the meshless discretizations. It is seen that meshless models have larger bandwidths, profiles, maximum frontwidths, and the root-mean-square wavefronts. Therefore, structural matrices resulting from FE discretizations are sparser.

 

## 7. CONCLUSIONS

In this article nodal connectivity and invertibility of matrices for element-free Galerkin method are studied. The node connectivity of meshless models is compared with that of the finite-element method. Similarities and differences are pointed out. It is explained that, in contrast to the finite-element method, we cannot be sure about the invertibility of structural matrices. In a finite-element model, as long as the essential boundary conditions of the structure are enough, the structural matrices are mathematically invertible. However, for meshless models, we have to choose domains of influence large enough to satisfy the basis. The appropriate sizes of the domains of influence are configuration dependent. For practical problems this is not an issue and we can have non-singular structural matrices by choosing $2 \leqslant d_{\mathrm{m}} \leqslant 4$. Structural matrices resulting from finite-element discretizations are sparser than matrices resulting from meshless discretizations as is confirmed by our numerical analysis.

Some associated graphs are defined for meshless models and it is shown that one of them is always a connected graph while the others may be disconnected graphs. Associated graphs are defined for coupled finite-element meshless methods. Using the associated graphs, algorithms are proposed for nodal ordering of meshless models and coupled finite-element meshless models. The associated graphs are compared numerically. Like most ordering problems, ordering for meshless models is configuration-dependent and nothing conclusive can be said about the superiority of a specific associated graph.

## REFERENCES


1. Lucy LB. A numerical approach to the testing of the fission hypothesis. *The Astronomical Journal* 1977; **82**(12):1013–1024.
2. Sulsky D, Chen Z, Schreyer HL. The application of a material spatial numerical method to penetration. In *New Methods in Transient Analysis*, Smolonski P, Liu WK, Hulbert G, Tamma K (eds). ASME, PVP vol. 246/AMD, 1992; **143**:91–102.
3. Nayroles B, Touzot G, Villon P. Generalizing the finite element method: diffuse approximation and diffuse elements. *Computational Mechanics* 1992; **10**:307–318.
4. Duarte CA, Oden JT. H-p clouds—a h–p meshless method. *Numerical Methods for Partial Differential Equations* 1996; 1–34.
5. Babuška I, Melenk JM. The partition of unity finite element method. Technical Report BN-1185, Institute for Physical Science and Technology, University of Maryland, 1995.
6. Liu WK, Oberste-Brandenburg C. Reproducing kernel and wavelet particle methods. In *Aerospace Structures*: *Nonlinear Dynamics and System Response*, Cusumano JP, Pierre C, Wu ST (eds). AD 33, ASME, 1993; 39–56.
7. Liu WK, Chen Y. Wavelet and multiple scale reproducing kernel methods. *International Journal for Numerical Methods in Fluids* 1995; **21**:901–931.
8. Liu WK, Jun S, Zhang YF. Reproducing kernel particle methods. *International Journal for Numerical Methods in Engineering* 1995; **20**:1081–1106.
9. Belytschko T, Lu YY, Gu L. Element-free Galerkin methods. *International Journal for Numerical Methods in Engineering* 1994; **37**:229–256.
10. Lu YY, Belytschko, Gu L. A new implementation of the element free Galerkin method. *Computer Methods in Applied Mechanics and Engineering* 1994; **113**:397–414.
11. Krongauz Y, Belytschko T. Enforcement of essential boundary conditions in meshless approximations using finite elements. *Computer Methods in Applied Mechanics and Engineering* 1996; **131**:133–145.
12. Cuthill E, McKee J. Reducing the bandwidth of sparse symmetric matrices. *Proceedings of the 24th National Conference ACM*, 1969; 157–172.
13. Kaveh A. Application of topology and matroid theory to the analysis of structures. *Ph.D. Thesis*, IC, London University, 1974.
14. Kaveh A. Ordering for bandwidth reduction. *Computers and Structures* 1986; **24**:413–420.
15. Cassell AC, de Henderson JC, Kaveh A. Cycle bases for the flexibility analysis of structures. *International Journal for Numerical Methods in Engineering* 1974; **8**:521–528.


 

16. Kaveh A, Rahimi Bondarabady HA. Ordering for wavefront optimization. *Computers and Structures* 2000; **78**:227–235.
17. Fenves SJ, Law KH. A two-step approach for finite element ordering. *International Journal for Numerical Methods in Engineering* 1983; **19**:891–911.
18. Sloan SW. An algorithm for profile and wavefront reduction of sparse matrices. *International Journal for Numerical Methods in Engineering* 1986; **23**:239–251.
19. Livesley RK, Sabin MA. Algorithms for numbering the nodes of finite element meshes. *Computers Systems and Engineering* 1991; **2**:103–114.
20. Kaveh A. A connectivity co-ordinate system for node and element ordering. *Computers and Structures* 1991; **41**:1217–1223.
21. Kaveh A, Behfar SMR. Finite element nodal ordering algorithms. *Communications in Numerical Methods in Engineering* 1995; **11**:995–1003.
22. Kaveh A, Roosta GR. Comparative study of finite element nodal ordering methods. *Engineering Structures* 1999; **20**:86–96.
23. Lancaster P, Salkauskas K. Surfaces generated by moving least-squares methods. *Mathematics of Computation* 1981; **37**:141–158.
24. Belytschko T, Krongauz Y, Organ D, Fleming M, Krysl P. Meshless methods: an overview and recent developments. *Computer Methods in Applied Mechanics and Engineering* 1996; **139**:3–47.
25. Dolbow J, Belytschko T. An introduction to programming the meshless element free Galerkin method. *Archives in Computational Mechanics* 1998; **5**(3):207–241.
26. Belytschko T, Organ D, Krongauz Y. A coupled finite element-element-free Galerkin method. *Computational Mechanics* 1995; **17**:186–195.
27. Sloan SW. A fortran program for profile and wave front reduction. *International Journal for Numerical Methods in Engineering* 1989; **28**:2651–2679.
28. Kaveh A. *Structural Mechanics*: *Graph and Matrix Methods*, 2nd Edition. Research Studies Press, Wiley: New York, 1995.
29. Kaveh A. *Optimal Structural Analysis.* Research Studies Press, Wiley: UK, 1997.

 